# μ-SLS of Metals: Design of the powder spreader, powder bed actuators and optics for the system

N.K. Roy*and M.A. Cullinan*
*Department of Mechanical Engineering, The University of Texas at Austin, TX 78712

## Abstract

Nanopowders have a tendency to form agglomerates due to high surface energy and the presence of attractive van der Waals forces. To overcome this problem, we present a powder spreading mechanism design that can alleviate this phenomenon by using vibration compaction to produce a uniform powder distribution in the bed. Most SLS machines employ either a roller or a blade to spread the powder over the powder bed. However, in order to achieve layer thicknesses of few microns, a new design for the spreading mechanism which includes a combination of a precision blade and a precision roller is employed. Also, the design of a linear actuating system for displacing the powder bed with resolution of few tens of nanometers is presented for the μ-SLS system. Finally, the paper presents a novel optical system that can drastically increase the throughput of the system .The detailed design of these systems are presented in this paper.

## Introduction

Laser sintering is an additive manufacturing technology employing a high power laser to fuse the metal powder into a mass that has a desired 3-dimensional shape. The laser selectively scans and fuses powder material on the surface of the powder bed based on the previously generated CAD file. After one layer is scanned, the powder bed is lowered by one layer thickness, creating a new layer that is scanned. The process is repeated until the part is completed[1].

The smallest feature sizes that the commercially available sintering machines can achieve is of the order of hundreds of microns and this study is focused towards designing a system to achieve 1μm feature sizes[2]. To get that feature size, it is required to use particles smaller than the feature size and hence, NPs were the first choice for the sintering . Since they have a very high surface area to volume ratio, oxidation becomes unavoidable in contact with air and thus, a high vacuum is required for sintering the powders. Traditionally, the spreading mechanism consisted of a counter rotating roller which would sweep across the powder bed spreading powder layer by layer but with the problem of agglomeration and very low density of nanopowders, this study presents a spreader design which consists of two stages to overcome the agglomeration effects and spread the powder uniformly in a layer. Another drawback with very small feature sizes is that the throughput of the process becomes very low using a conventional optical system and in order to increase the throughput of the process, we decided to use Texas Instruments' Digital Micro-mirror Devices (DMDs) for our system in conjunction with the fiber laser. The study presents an analysis of the maximum temperature that the pixels that can reach during operation and some calculations have been performed to estimate the throughput of the process using the DMDs also.

## Background

The SLS process was developed and patented at the University of Texas at Austin. DTM Corporation was founded in 1987 to commercialise the SLS technology, and shipped its first commercial machine (Sinterstation 2000) in 1992[3]. In the year 2002 selective laser micro sintering was developed by Laserinstitut Mittelsachsen e.V[4]. It is a modification of selective laser sintering and has been successfully employed since then to generate metal micro parts with a structural resolution of $< 12\mu m$[2]. Since 2005, new powder coating techniques have been tested to improve the powder layer density. A variety of different rakes has been experimented with among others the approved ring shaped blade [5] has been supplied with compressing rollers, and additional force supported rakes have been tested to achieve denser powder packing [6].

## A. Design of Actuation System for the piston-cylinder arrangement

The design of the actuation system should be such that the minimum step size is 10 times (or more) smaller than the minimum feature size ($1\mu m$) so that the control over thickness of the layer is more accurate. Thus, ball screw/lead screw- stepper motor assemblies were chosen to move the pistons up and down with a resolution of *40nm*.

**a) Main Cylinder and piston**: In order to generate step movements of *100nm* (or lower), a stepper motor integrated with either a precision ball screw or a precision lead screw was the primary choice for actuation. Generally, the stepper motors have a resolution of 200 or 400 steps/revolution . With a *1mm* pitch lead screw, the smallest step size that one can get using the system is $1/400*1mm=2.5\ \mu m$ per step which is higher than what is required for this application and, hence the need for micro-stepping. Therefore, STM23Q-2AE Integrated Stepper Drive from Omega Engineering, Inc was chosen for the main piston actuation. Furthermore, it was decided to use ball screw instead of lead screw because ball screws have ball bearings in them which eliminates the friction between the nut and screw while lead screws do not. This increases the life of the screw and also improves the accuracy and repeatability of the step sizes over time. Some basic torque calculations for the screw and motor torques:

$$T_{total} = T_{friction} + T_{acceleration} \quad (1)$$

$$T_{friction} = F/(2*\pi*p*e) \quad (2)$$

$$F = \mu_r * W \quad (3)$$

$$J_{load} = W/(2*\pi*p)^2 \quad (4)$$

$$J_{leadscrew} = \pi*\rho*L*R^4/4 \quad (5)$$

$$T_{acceleration} = (1/g)*(J_{load}/e + J_{leadscrew} + J_{motor})*\omega/t \quad (6)$$

$$\omega = \theta/t \quad (7)$$

*where F= frictional force (oz), p=pitch (revs/in), e= ballscrew efficiency, $\mu_s$= coefficient of rolling friction, W=weight of the load (oz), $J_{load}$= Inertia due to load , $J_{leadscrew}$= inertia of the leadscrew, L=length of the screw (in), R=radius (in) and $\rho$= density (oz/in$^3$), $J_{motor}$= inertia of the motor, g =acceleration due to gravity (in/s$^2$), $\omega$= angular velocity (rad/s), $\theta$= angular displacement (rad) and t=time (s)*

For the motor and screw selected above, the values of the parameters are: *p=25.4 revs/in, e=0.96, $\mu_r$=0.003-0.01, W=35.274 oz (1 kg at max. including the weight of the piston and powder), $\rho$= 4.48 oz/in$^3$, L=10 in, R=6mm, $\theta$= 25.4*2*$\pi$= 159.59 radians and t=10s.* In other words, it is assumed that the ball screw covers a distance of *1inch in 10s* which is the higher limit on the angular speed. There is no way that the angular speed can be higher than this as the step size is not going to be more than a few μm. With the above stated parameters , the value of total torque comes out to be *0.0205 oz-in* which is 3 orders of magnitude smaller than the max. torque of the motor and hence, the motor selected should be fine for the application.

Since the motor end and ball screw have different nominal diameters, so a flexible coupling from Rocom Corporation which matches the diameters of the motor and the ball screw was used as an interface between the two components . Flexible couplings accommodate relative movement between the drive-train components due to any temperature change or pressure change and permit end movement of the shafts without placing unwanted stresses on bearings and seals.

**b) Feeder Cylinder and Waste Cylinder:** For these cylinders, high precision motion is not the objective and hence, normal lead screws could be employed for their operation. A 23MDSI106S-00-00 - Integrated Stepper Motor/Driver/Indexer from Anaheim Automation, Inc was used as the stepper motor in conjunction with Lead Screw- WDG-F-L-R-025-039 from Haydon Kerk Motion Solutions and a Aluminum Helical Flexible Shaft Coupling-Set Screw, *1/4" x 1/4"* Diameter Shaft, *7/8"* Long, *5/8"* OD from McMaster Carr.

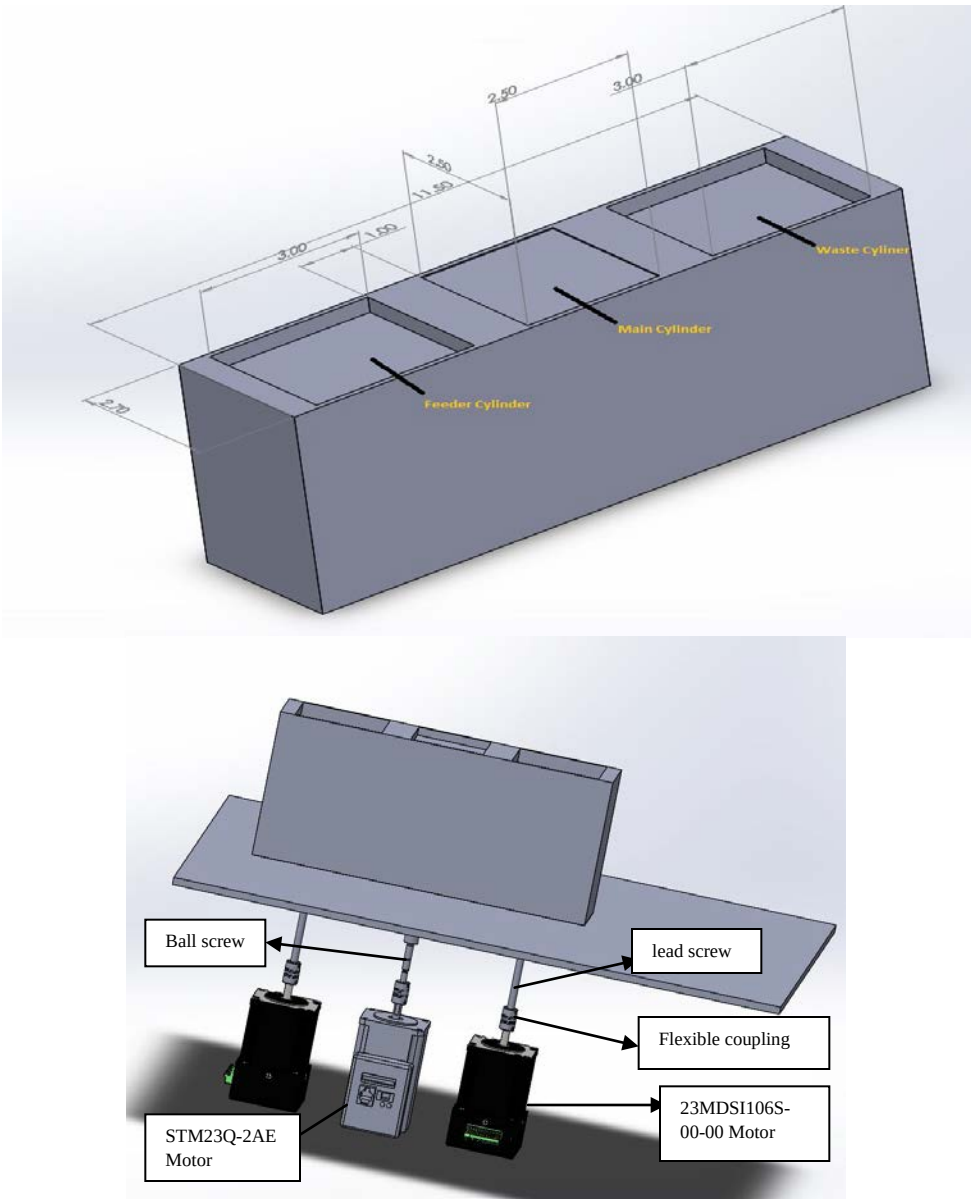


Figure 1. a)CAD model with dimensions of the main, waste and feeder cylinder and piston arrangements b)CAD model of the actuation assembly for the cylinder and piston arrangement

## B. Spreader System

Nanopowders have a tendency to form agglomerates because of their high surface energies due to high surface area/volume ratios. Also, the attractive van der Waals forces start dominating the gravitational forces. As a result of agglomeration, the packing density and uniformity of the powders in the layer declines. Thus, it is required to minimize the agglomeration as much as possible. The particles are surface treated to reduce this problem but it is beneficial to use some raking procedure that further breaks these agglomerates and compacts the layer.

Thus, to overcome this problem, a powder spreading mechanism has been designed to alleviate this phenomenon by using vibration compaction to produce a uniform powder distribution in the bed. Most SLS machines employ either a roller or a blade to spread the powder over the powder bed. However, in order to achieve layer thicknesses of few μm, a new design for the spreading mechanism which includes a combination of a precision blade and a precision roller is employed. The powder spreading procedure consists of two stages for raking the powder layer on the bed:

1. Spreading the powder layer using a precision blade

2. Compacting the layer of the powder using a vibrating counter rotating precision roller.

**Selection of Components**

**1. Precision Blade and Precision Roller**: First, a precision blade scrapes over the surface and creates a layer of the powders. Next, a vibrating counter -rotating roller sweeps over the surface to break down the agglomerates and helps in increasing the compactness of the powder. The carriage for precision roller has a voice coil in it which generates the vibrations in the roller.

Also, in order to control the displacements of the roller during vibration, both the blade and the roller are spring loaded so that a constant force is pushing it down and they do not lose contact with the layer anywhere during operation.

a) Precision Blade- A white carbon steel blade (coated with both ceramic and PTFE) is suited for solvent based coating solutions and inks. So, the blade is flexible with the choice of dispensing material (either powders or inks ). Due to nanoparticles, the blades could easily get damaged due to abrasion and hence, the coatings are used to increase the abrasion resistance of the blades. The straight edge shape of the blade is also effective for applications where the doctor blades can get quickly abrasion damaged.

In addition to this, there will also be a precision edge finished backup blade (presser) to improve the wiping effect of the precision blade. A straight edge white carbon steel blade (SKNF) with *0.15mm* thickness from Eco Blade,Inc Japan has been employed as the main blade, along with a SUS301 straight edge ,thickness -*0.15mm* as the backup finishing blade[7].

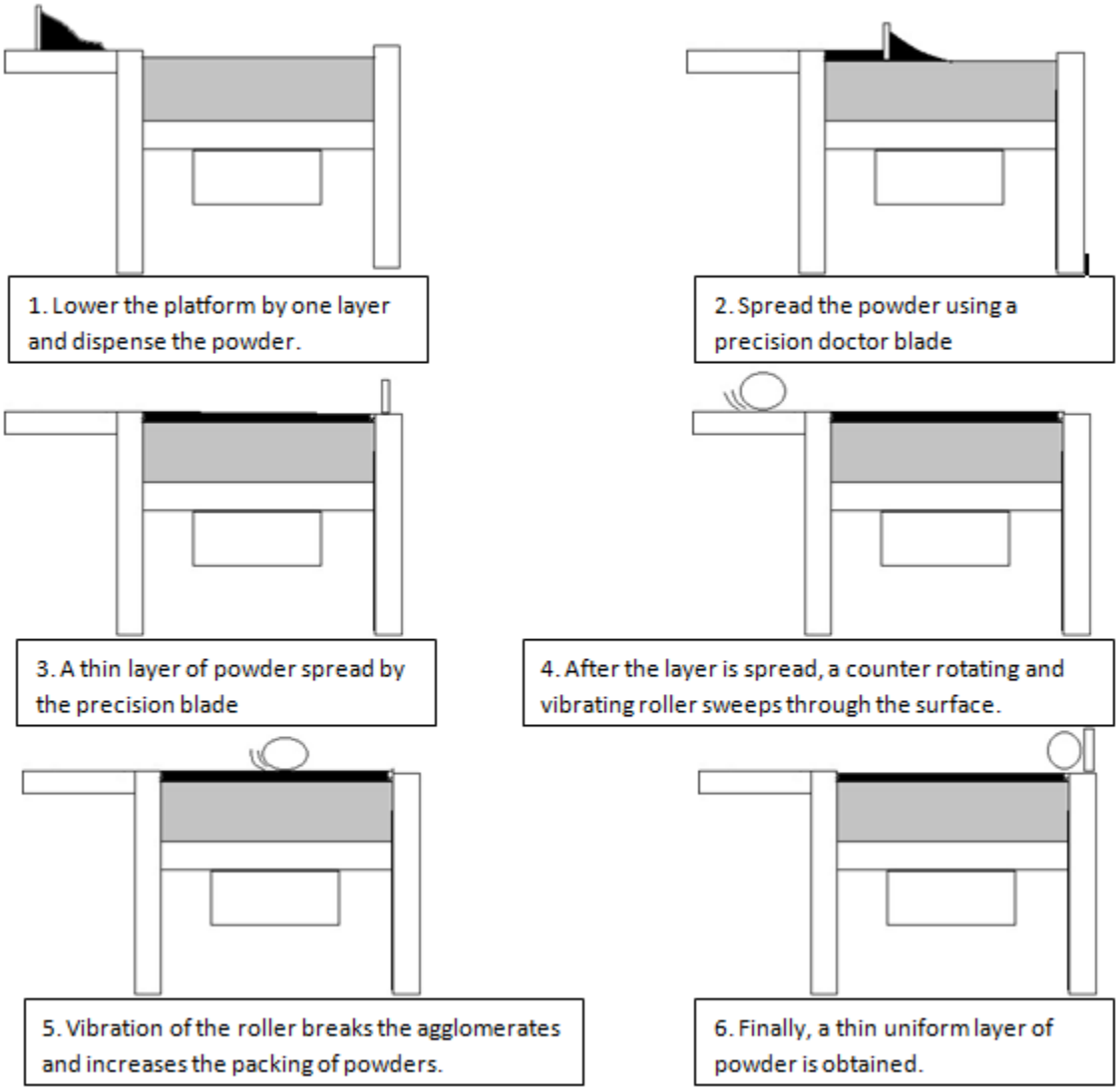


Figure 2. Schematic of the powder spreading mechanism

b) Precision rollers: It was decided to use a counter-rotating roller which is vibrating to increase the packing density in the powder bed. Since the average particle size is around a hundred nanometers, so the roller's surface roughness should definitely be lower than that so that the particles are not clinging to the roller's surface i.e. the surface roughness of the roller should be at most few tens of nanometers. For this, custom made rollers from Bal-Tec, Inc. , California , USA have been selected. The rollers have a surface finish of *2 micro-inch(50.8nm*) and are precision lapped which gives a tight range on the roundness of the roller.

For the motion of blade and roller, timing belt and pulley transmission is better over other actuation mechanisms like rack and pinion, chain and sprocket, v-belt and pulley etc. due to its low cost, minimal vibration and noise, shock absorbent for load fluctuations, clean (no

lubrication), virtually no elongation, no need for tensioning devices , no slippage and so on [8]. Selection of rails, carriages, timing belts , pulleys and driving motors is critical for a smooth operation of the blade and the roller over the powder bed.

**2. Rails and Guides:** The length of the rails is dictated by the sizes of the main cylinder and feeder and waste cylinders which in turn depends upon the size of the working area that we want. For this machine, based on a working area of *2" by 2"*, the cylinders' sizes are determined. and after sizing the cylinders, a rail and guide system which is *18.7"* long and *4.97"* wide was selected for guiding the roller and precision blade. The carriage (Fig. 3) should have mounting holes on its top so that the carriers (Fig. 7) for the blade and the roller could be mounted on it.

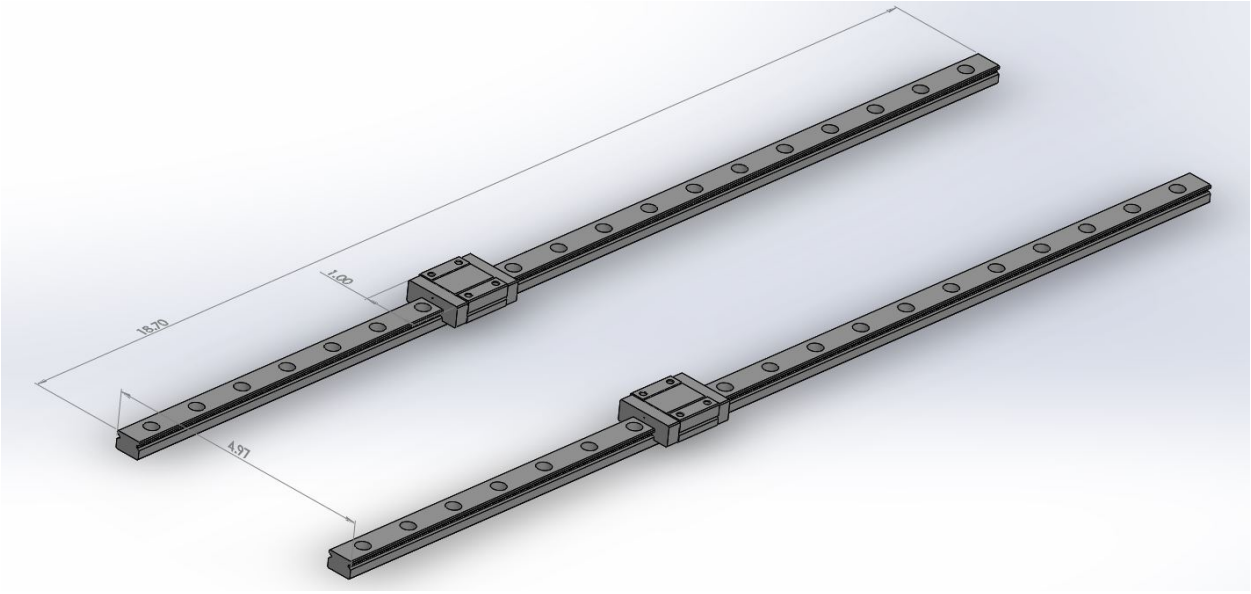

Figure 3. CAD model of the rails and guides

**3. Belts and Pulleys:** As discussed earlier, timing belt and pulley was chosen over v-belts or flat belts because of its precision registration and timing , no slippage, no elongation and these systems are best suited for use with stepper motors and where precise positioning is required.

Since the total length to be traversed comes out to be *18.7"*, so the following were chosen:1. Belt-Trapezoidal Tooth Neoprene Timing Belt (*.200"* Pitch, Trade Size 400xL, *40"* Outer Circle, *1/4"* Wide) from McMaster Carr (6484K513) 2. Pulley- L and H Series Timing Belt Pulley-XL-Series, Fit *1/4"& 3/8"* Wide Belt, *1.12"* OD, 14 Teeth (6495K714)

Apart from belt and pulley, belt's motion has to be transferred to the carriers for roller and blade. That is achieved using a clamp plate for the belt. The clamp plate (Fig.4) has mounting

holes on its top and the carrier can be mounted to the plate using standard nuts and bolts

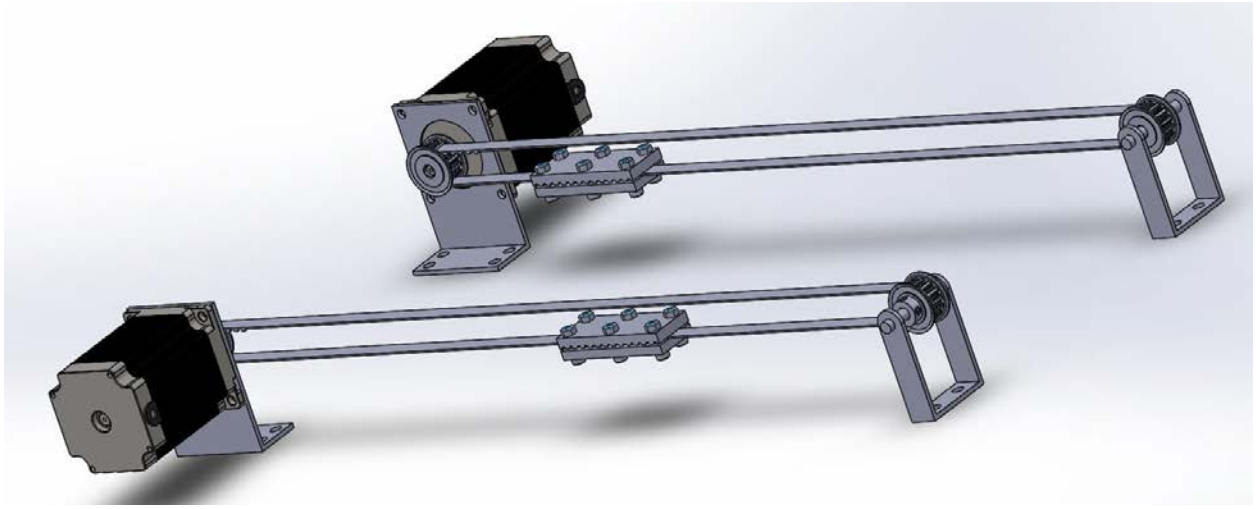

Figure 4. CAD model of the belt, pulley and mounts for motors and pulley

**4. Motors** : The motors for driving these pulleys have to be vacuum compatible. Another important consideration is that the shaft diameter of the motor should match with the minimum bore diameter pulley that we can get for the belt. The motor VSS 56.200.1.2 from Phytron,Inc [9] were chosen for the application. Calculations for the torque requirements are shown below.

$$T_{Total} = T_{load} + T_{Pulley} + T_{belt} + T_{motor} + T_{friction}$$

$$= (1/g) * (J_{load} + J_{pulley} + J_{belt} + J_{motor}) * \omega/t + T_{Friction} \quad (8)$$

$$J_{load} = W_{load} * R^2 \quad (9)$$

$$J_{pulley} = W_{pulley} * R^2 * 2/2 \text{ (because there are two pulleys)} \quad (10)$$

$$J_{belt} = W_{belt} * R^2 \quad (11)$$

$$T_{friction} = F * R \quad (12)$$

$$\omega = V/R \quad (13)$$

*where, T and J have their usual meanings as stated above, $W_X$= Weight of the element X (oz), R=radius of the pulley (in), F= frictional force, V= Velocity of the belt (in/s), ω= angular velocity (rad/s). Assuming that the whole 20" distance is traversed in 10s then the velocity comes out to be 2inch/s. Values of other parameters for calculations are listed below.*

$W_{load}$*= 1kg= 35.274 oz* (This is the maximum possible weight of the load as the carrier is mounted on the rails, so the weight of the carrier is not on the pulley directly).
$W_{Pulley}$*= 0.7152 oz* (assuming a cylinder with OD of the pulley as the diameter and the thickness of the pulley as the height.
$W_{Belt}$*= 0.8887 oz* (assuming it as a cuboid), *R= 0.565 in,* $J_{Motor}$*= 0.9294 oz*in*$^2$ . For estimating

the frictional force, let's assume that the torque due to the frictional force be the same as sum of other torques- though it is much lower in real systems (between 1/8-1/30 of the total torque).

Using these parameters, $T_{Total}$*=0.023229oz*in=0.1645 mN-m*, which is way less than the holding torque of the motor which is *420 mN-m*. Hence, the motor selected should be suitable for our application. Though, a motor with lower torque specification could have been selected as well, however finding a pulley matching both the belt specifications and lower shaft diameter of the motor becomes extremely challenging and that's why the above mentioned motor was selected.

**5. Carriage for precision roller and precision blade**: The carriage design is based on following considerations.

a) Carriage is to be mounted on the clamp plates for the belts using standard nuts and bolts. This is achieved by using a top plate that acts as an interface between the clamp plate and the carriage plates for the blades and the rollers.

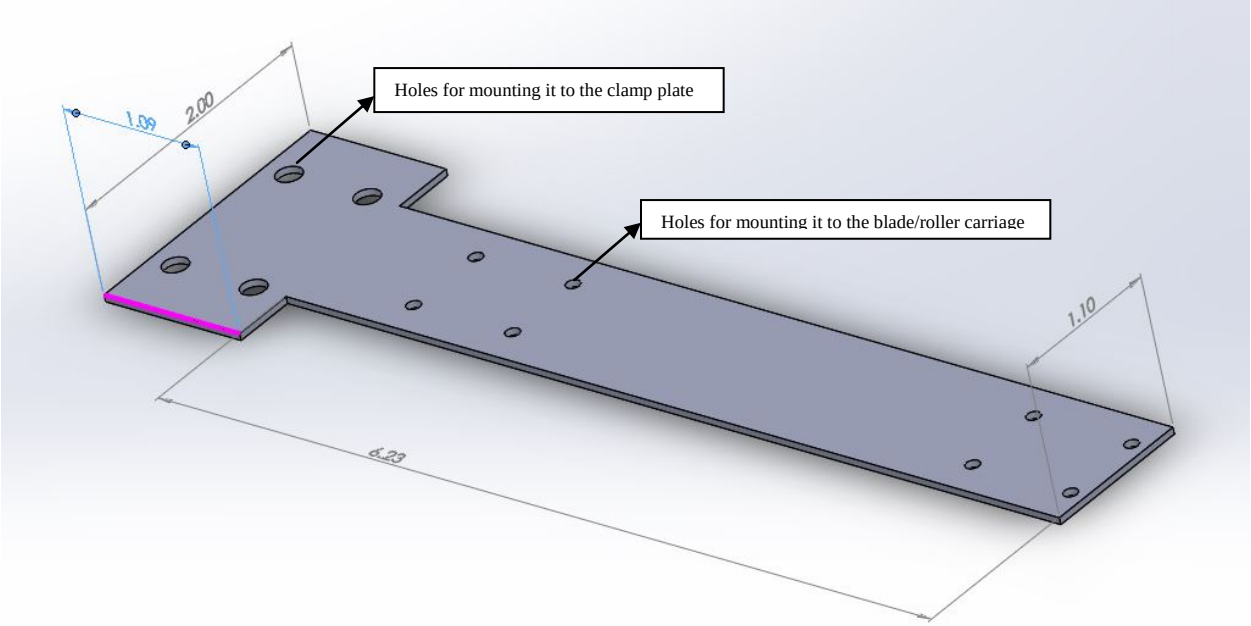


Figure 5. CAD model of the top plate

b) In order to use 10Xor even higher objective lenses, it is desired that the working distance for the lenses be as small as possible. Keeping that in mind, the carriages have been designed accordingly. The minimum working distance for this design is *1.08"(27.4mm)* which is within the working distance for a 10X objective lens. (for 10X Mitutoyo Plan Apo Infinity-Corrected Long WD Objective, the working distance is *33.5mm*)

c) The designs for carriages have slots for blades and roller bearings for rollers. Also, their walls have linear voice coil actuators which in combination with flexures will transmit very

low amplitude high frequency vibrations to the roller attached to the carriage. This operation is to be carried out after the precision blade has swept the surface.

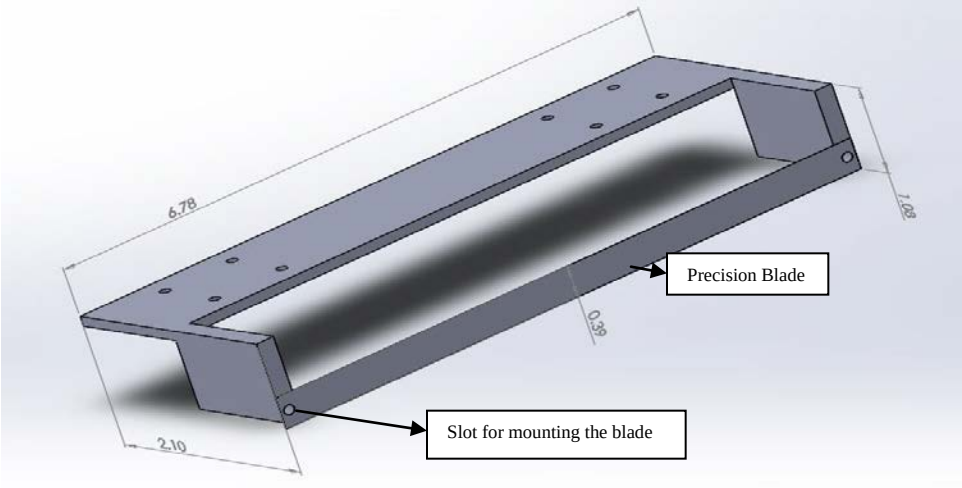


Figure 6. CAD model of the blade carriage and the blade- the holes are for mounting it onto the top plate

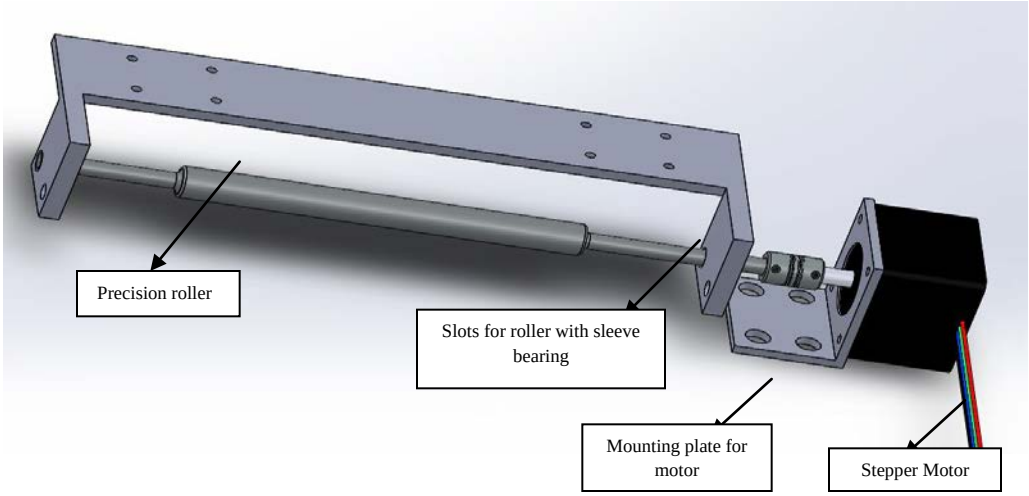


Figure 7. CAD model of the roller carriage and roller- slots for different roller sizes

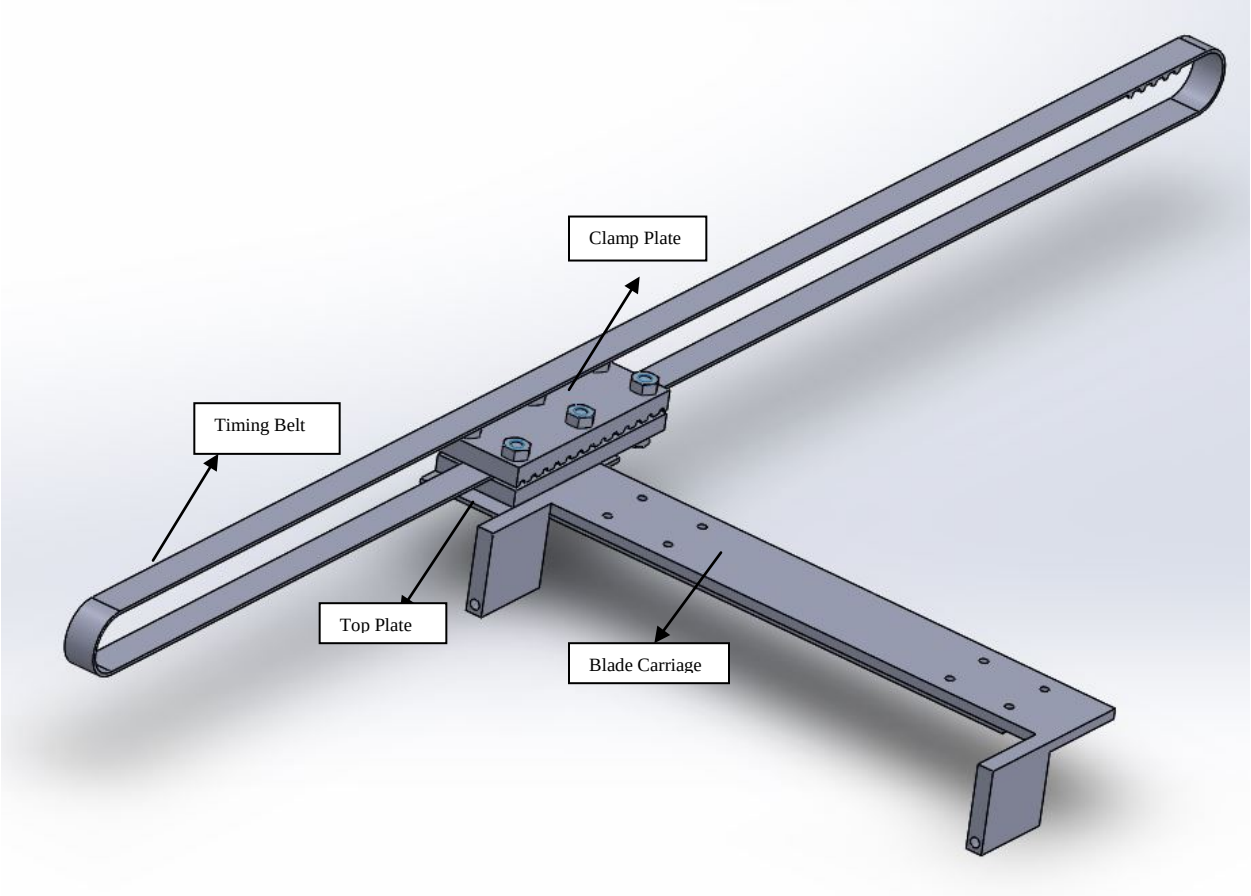


Figure 8. CAD model of Belt-Clamp Plate Sub Assembly

**6. Motor for counter-rotating the roller:** For counter rotating the roller, another vacuum compatible stepper motor VSS 32.200.1.2 from Phytron, Inc[9] is being used. Since, there are no minimum shaft diameter constraints, a motor with lower torque specification and a flexible coupling for motion transmission between the motor and the roller have been selected.

**7. Mounts for motors and pulleys:** All the motor mounts and pulley mounts are shown below in the sub-assembly.

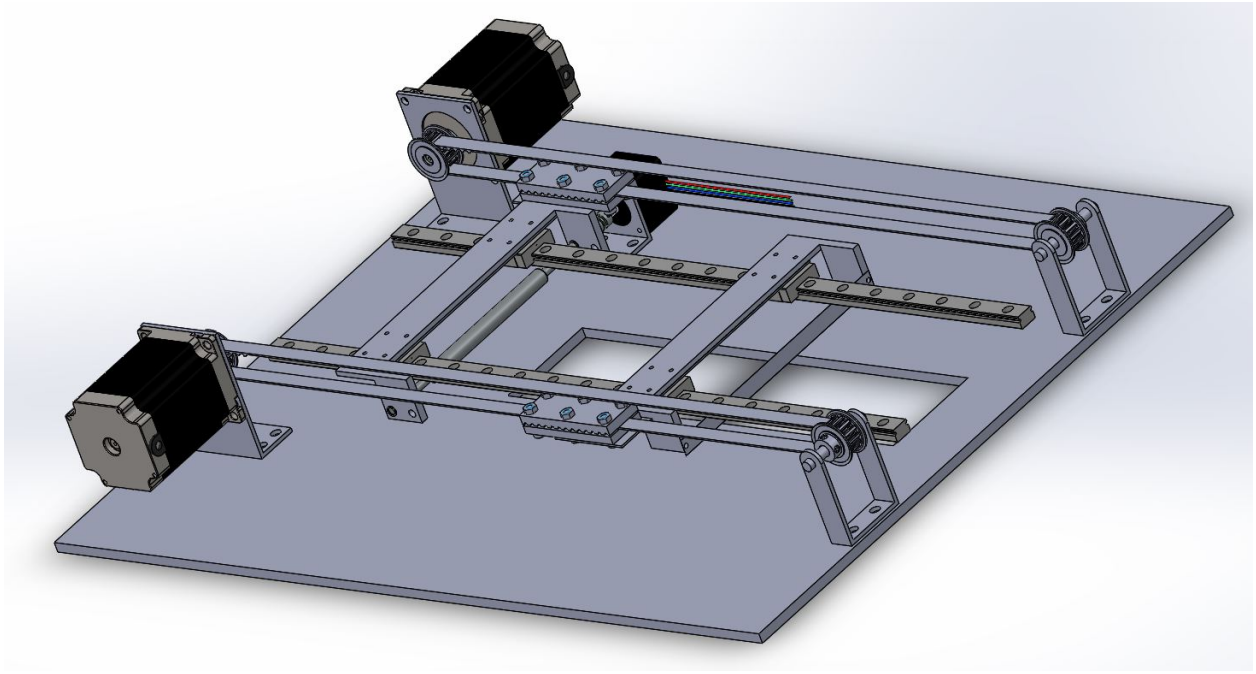

Figure 9. CAD model of the powder spreader sub assembly

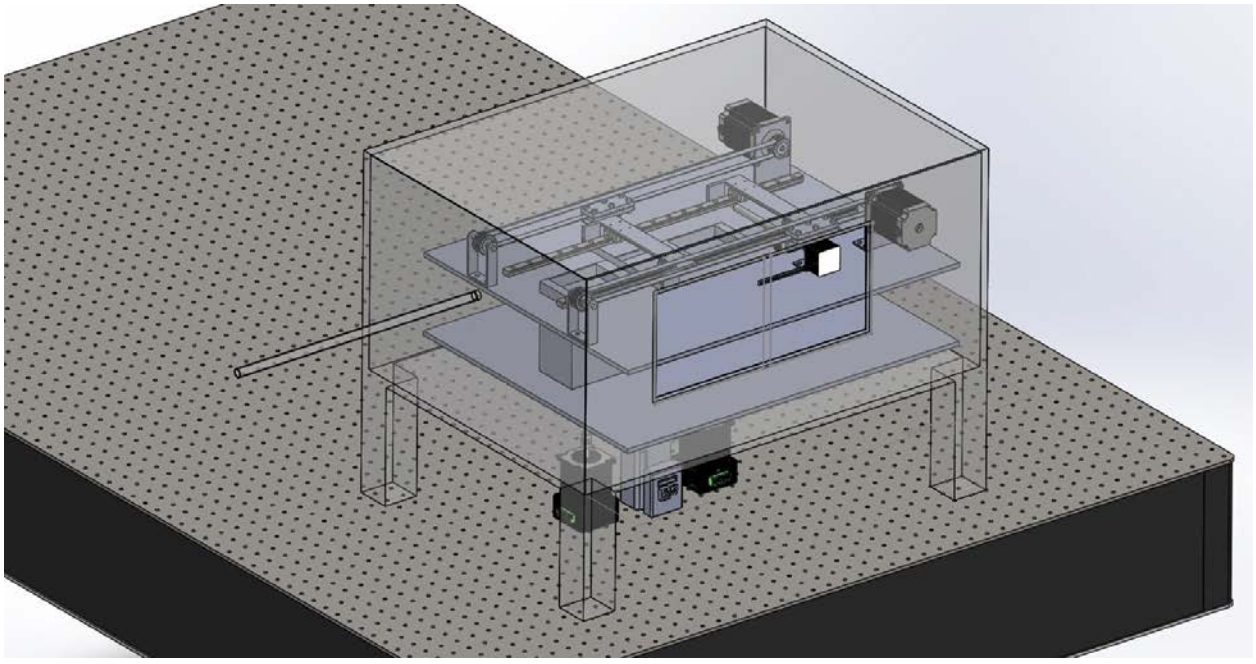

Figure 10. CAD model of the sub- assembly excluding the vacuum pump

## C. Vacuum system

High surface area to volume ratio of Cu NPs particles which makes these particles highly reactive. As a result, the particles can get oxidized very easily which will affect the properties of the sintered part. Thus, it becomes imperative to conduct the sintering in an inert environment or under vacuum where there are negligible chances of oxidation of the particles.

| | |
|---|---|
| Rough Vacuum | 100 to 0.1 Pa( 1to $10^{-3}$ torr) |
| Low Vacuum | 0.1-$10^{-4}$ Pa($10^{-3}$ to $10^{-6}$ torr) |
| High Vacuum | $10^{-4}$ to $10^{-7}$Pa ($10^{-6}$ to $10^{-9}$ torr) |
| Ultra-High Vacuum | lower than $10^{-7}$ Pa ($10^{-9}$ torr and below |

Table 1. Different vacuum qualities

Using low vacuum, one still gets traces of oxygen inside the compartment and that can oxidise the NPs . Thus, it is better to use high vacuum for this sintering setup. Based upon the vacuum requirements for the setup, there were two options for the vacuum pump- either to use a diffusion pump or a turbomolecular pump

a) Diffusion Pump- Pumping effect is based on diffusion of gases into a gas free high speed vapor jet which are obtained by boiling a high molecular weight , low vapor pressure, no-reactive fluid like oil[10]. But there are chances of oil vapor leaking into the chamber and thus, contaminating the powders.

b) Turbo-Molecular pumps- It consists of a stack of rotors with multiple angled blades that rotate with high speeds between a stack of stators which forces the gas out through the exhaust[10]. Since, they do not use any fluid, they do not introduce any contaminant into the chamber and thus, it was decided to use a turbo pump along with a backing pump. The backing pump first creates a rough vacuum inside the chamber and then, the turbo molecular pump is used to create a high vacuum.

For this purpose, a vacuum chamber which can withstand high vacuum would be required. Following is an image of the designed vacuum chamber.

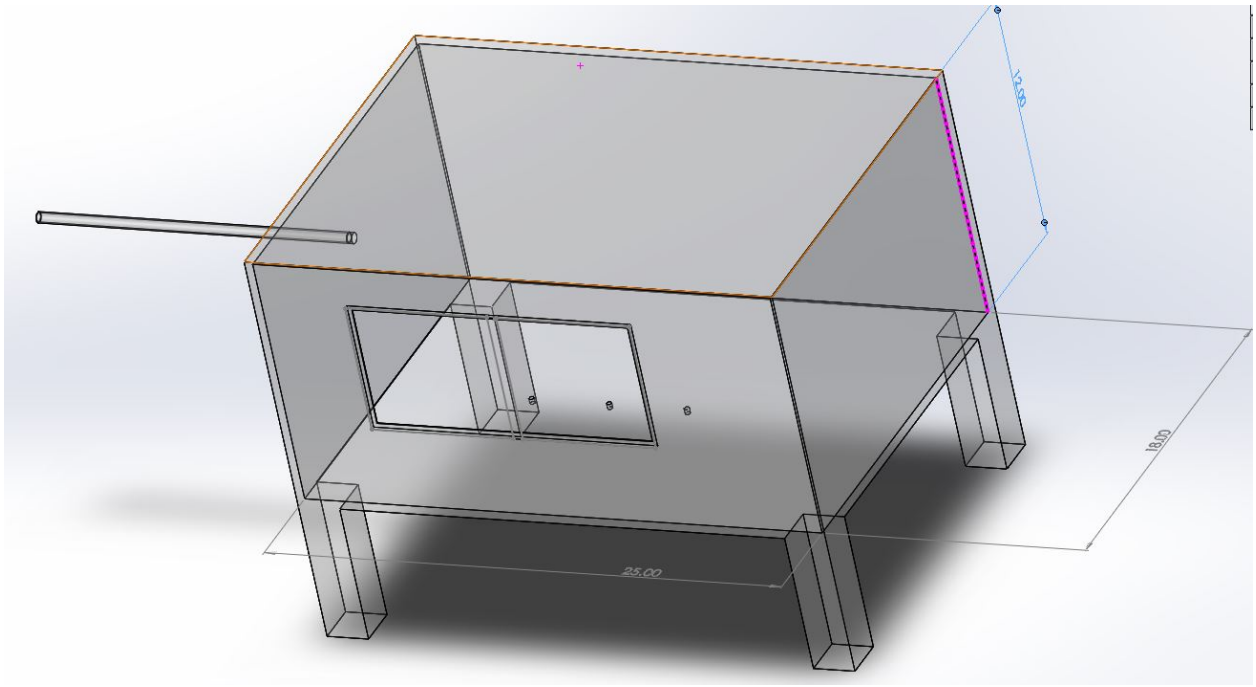


Figure 11. CAD model of the vacuum chamber with an opening for loading the powders

**Calculations for Pumping speed**

Volume of the container to be vacuumed= *25"*18"*12" =0.08849m$^3$ =88.49litres*

Ultimate Pressure Desired= *$10^{-5}$mbar*

Assume no leaks through valves or walls and we want to achieve the ultimate pressure in 2 minutes, then

$$S_{eff} = (V/t)*\ln(p_i/p_f) \qquad (14)$$

*where V= volume of the chamber (m$^3$), t= time(s), $p_i$= initial pressure= 1013 mbar, $p_f$= final pressure*

Here, *$S_{eff}$=0.014 m$^3$/s= 13.59 l/s = 48.15 m$^3$/hr* which is a high pumping speed requirement. But if a backing pump is employed to first create a rough vacuum , say *$10^{-2}$ torr= $1.3*10^{-2}$ mbar*, then

Effective Pumping Speed for turbo-pump, *$S_{eff}$= 5.28 l/s*. This addition of a backing pump leads to a considerable decrease in the effective pumping speed required.

$$\text{Pumping Speed for backing pump, } S_V = p_A*S_{eff}/p_V \qquad (15)$$

$$= 0.0686 \text{ l/s} = 0.247 \text{ m}^3\text{/hr},$$

*where $p_A$= inlet pressure at the turbopump (in this case, it is $1.3*10^{-2}$ mbar), $p_V$= maximum permissible backing pressure= 1mbar (for MVP 070)*

Based on the calculations above, Hi Cube Classic MVP 040 which uses a Hi Pace 80 Turbopump (*67 l/s pumping speed* ) and a MVP 040 diaphragm pump as the backing pump ($2.3m^3/h$)[11] was selected. Using this, one can reach a pressure of $10^{-5}$ *mbar* in a *100 litre* compartment in *978s*. For the compartment designed for the setup whose capacity is *88.49 litres*, it should take *865.43s* to get to a pressure of $10^{-5}$ *mbar*.

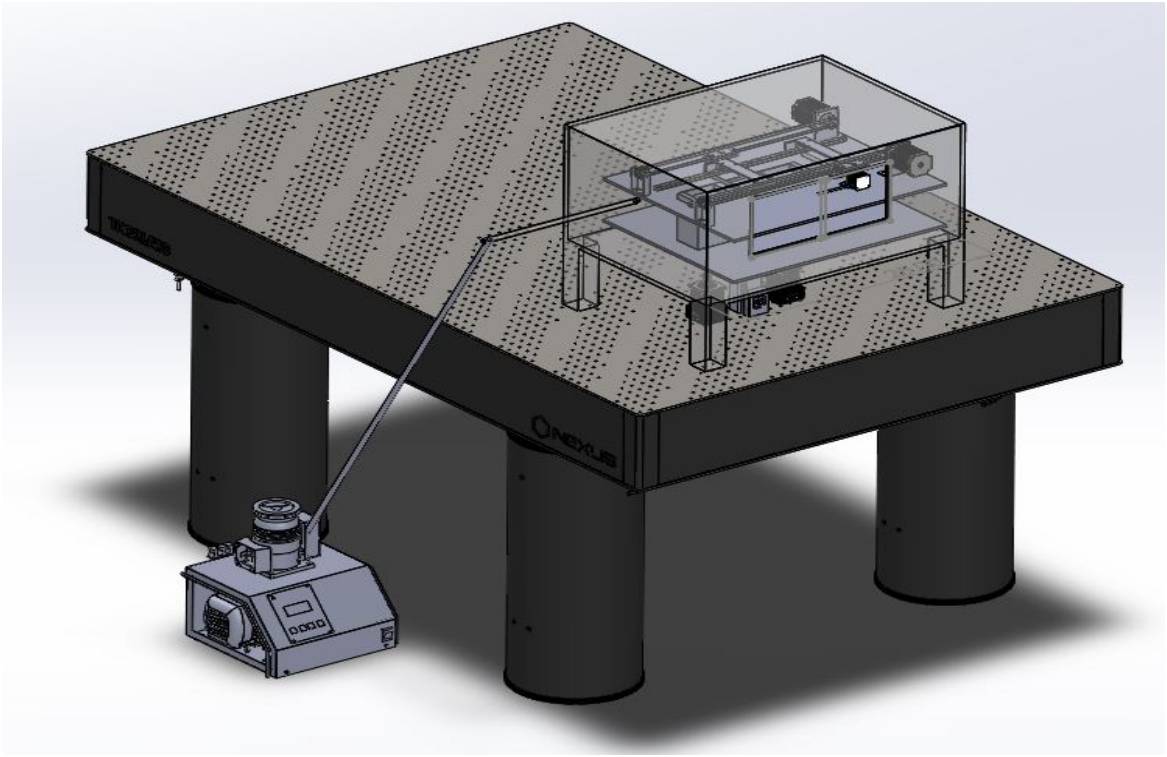

Figure 12. CAD model of the final assembly resting on a vibration isolation table from ThorLabs,Inc

## D. Laser and Optics

Traditionally, the optics for an SLS system includes beam expanders, some reflection mirrors, a 3-axis dynamic scanner or an $f_\theta$ lens and an x-y galvano mirror. Getting down to a feature size of *1 $\mu m$* will need high focusing objectives and with all these optical elements over the powder bed, it becomes a challenging task to achieve very low working distance. Also, since the desired feature size is only *1 $\mu m$*, the throughput for the process will be pretty low if a traditional optical system that sinters one spot a time is employed for operation.

In order to increase the throughput of the process, it was decided to use a light engine CEL 5500 by Digital Light Innovations. CEL 5500 uses Texas Instruments DLP®5500 *0.55"* XGA chipset. The digital micromirror device (DMD) is optically efficient for wavelengths in the range *420-700nm*. The chipset consists of an array of 1024*768 aluminum micro-mirrors with

binary pattern rates upto *5000 Hz*. The micro-mirrors are *10 μm* by *10 μm* in size and are placed apart at a distance of *800nm*. So, we can see that one beam can be split into a total of 786432 beams with a feature size of *10 μm* [12]. That is a significant improvement in the throughput of the process than using a single beam to sinter one spot at a time. The laser beam from the laser can be fed into the light engine using a connecting fiber. Although, the throughput of the system has increased, the power requirements for the laser also increases considerably. And, it is also important to check that the aluminum mirrors are not damaged due to use of such high powered laser. A simplified model to estimate the energy required to sinter the nanoparticles has been developed. The model is useful in deciding the power levels to be used for the laser. Some assumptions for the model are:

1. The properties of the nanoparticles like the specific heat capacity and density are assumed to be the same as that of the bulk material.

2. It is assumed that the particles sinter at *10°C* below their melting point which is *1085 °C*. The sintering temperature for the powders depend upon a number of factors like density of the powders, its composition , particle size, morphology and sintering time. Based upon these factors, the sintering temperatures for Copper can vary widely but it is significantly lower than the melting point of the bulk. The most commonly used sintering temperatures are around *600-800 °C* but sintering has also been tried at temperatures as low as *250 °C* for prolonged time [13]. But, it is better to get an upper limit on the power requirements and hence, a sintering temperature very close to the melting point has been assumed.

3. All the laser energy is expended in raising the temperature of the particles i.e. there are no losses in the energy transfer to the surroundings or neighboring particles.

4. Absorptivity of the copper is assumed to be *0.59* [14]

5. Spot size diameter=*10 μm*, Layer Thickness= *1 μm*

6. The spot size is sintered in one pulse.

| | |
|---|---|
| Specific Heat Capacity of Cu($C_{p)}$ (J/kg-K) | 385 |
| $T_i$(° C) | 20 |
| $T_f$(° C) | 1075 |
| Heat of fusion of Cu(J/kg) | 205000 |
| Melting Point(° C) | 1085 |
| Density of Copper(ρ)(kg/$m^3$) | 8900 |
| Reflectivity (R) | 0.41 |
| Absorptivity | 0.59 |
| Diameter of the spot (D) (μm) | 1.00E-05 |
| Layer Thickness (h)(μm) | 1.00E-06 |

Table 2. Properties of Copper and spot size

**Governing Equation**

Pulse energy to sinter a spot size of diameter D and layer thickness, h in n pulses,

$$E_n = \rho*\pi*D^2*h*[C_P*(T_f-T_i)+l_f]/(4*n*(1-R)) \quad (16)$$

and, Average power, $P_{avn} = E_n * f$ (17)

*where f= repetition rate of the laser, ρ= density of the powders, $C_P$= Specific heat capacity of the powders, $l_f$= heat of fusion of the powders, $T_i$= initial temperature of the powder bed, $T_f$= sintering temperature of the powder bed and R= reflectivity of the powders.*

| | Pulse energy, $E_n$ (nJ) | | Repetition rate of the laser(KHz) | Average Power, $P_{av_n}$ (mW) | |
|---|---|---|---|---|---|
| Spot sizes (μm) | n=1 | n=10 | | n=1 | n=10 |
| | | | 5 | 2.405 | 0.2405 |
| D=10,h=1 | 481 | 48.1 | 20 | 9.62 | 0.962 |
| | | | 100 | 48.1 | 4.81 |
| | | | 5 | 0.02405 | 0.002405 |
| D=1,h=1 | 4.81 | 0.481 | 20 | 0.0962 | 0.00962 |
| | | | 100 | 0.481 | 0.0481 |

Table 3. Power estimates for different spot sizes and number of pulses to sinter the spot

Using a *100KHz* laser, say it takes 1000 pulses to sinter a spot size of *1 μm* with *1 μm* thickness then, minimum power of the laser to use the DLP 5500 in order to sinter a spot of *1 μm* using 1000 pulses at *100KHz* $=0.00481*10^{-9}*100*10^{3}*1024*768 = 378mW$. Based on the calculations above, and the fact that DLP 5500 is suited for lasers in the wavelength range *420-700nm*, Talon 532-20 laser from Spectra-Physics (Newport ) was selected. It emits a laser beam with a wavelength of *532nm* at a repetition rate of *100 KHz* with an average power of *18W*. The maximum pulse duration of the laser is *25 ns*.

It is also important to check if this laser can damage the aluminum mirrors in the DLP 5500 chipset during operation. There are two important criteria to be met for using the DLP 5500 a) The average power density cannot exceed the specification of $25W/cm^2$ . b) The temperature of the pixels should not exceed a temperature of *150 °C* as the aluminum mirrors may get damaged beyond that[15] . So, it is important to check that these conditions are met for the laser selected above and the calculations have been shown below.

1. Average Power Density should not be greater than $25W/cm^2$. The laser can provide a maximum power of *18W* at *100KHz* . It is assumed there is no loss of energy between the time when energy comes out of the source and the time when it hits the mirror in order to get an upper limit on the value of average power density.

| | |
|---|---|
| No. of mirrors along the length | 1024 |
| No. of mirrors along the width | 768 |
| Mirror pitch(m) | 1.08E-05 |
| Max. Laser Power being used(W) | 18 |
| Repetition rate (f)(in Hz) | 1.00E+05 |
| Pulse Width of laser (s) | 2.50E-08 |
| Duty Cycle (%) | 2.50E-01 |

Table 4. Properties of CEL 5500 Light engine

Using the values of the parameters stated above,

Average Power density= Power/Total area of the mirror chipset (18)

$= 19.6\ W/cm^2$

and Peak Power density = Average Power Density/Duty Cycle (19)

$= 7.85\ kW/cm^2$

It is to be noted that the average power density $<25W/cm^2$ and hence, first condition is met.

2. Temperature of the micro-mirror.- The pixel temperature depends upon the array temperature and the rise above the array temperature i.e.

$$T_{Pixel}=T_{array}+\Delta T_{rise} \quad (20)$$

And, $$T_{array}= T_{ceramic}+T_{rise\ above\ ceramic} \quad (21)$$

Typically, the ceramic temperatures can reach upto *50-55 °C* and from the datasheet of CEL550 XGA S450, the temperature rise above ceramic can be *5 °C*[16]. So, the array temperature comes out to be *55-60 °C*.

In order to calculate the temperature rise of the pixel above array temperature, we can either use the temperature charts provided by TI or use the tables to estimate the temperature rise.

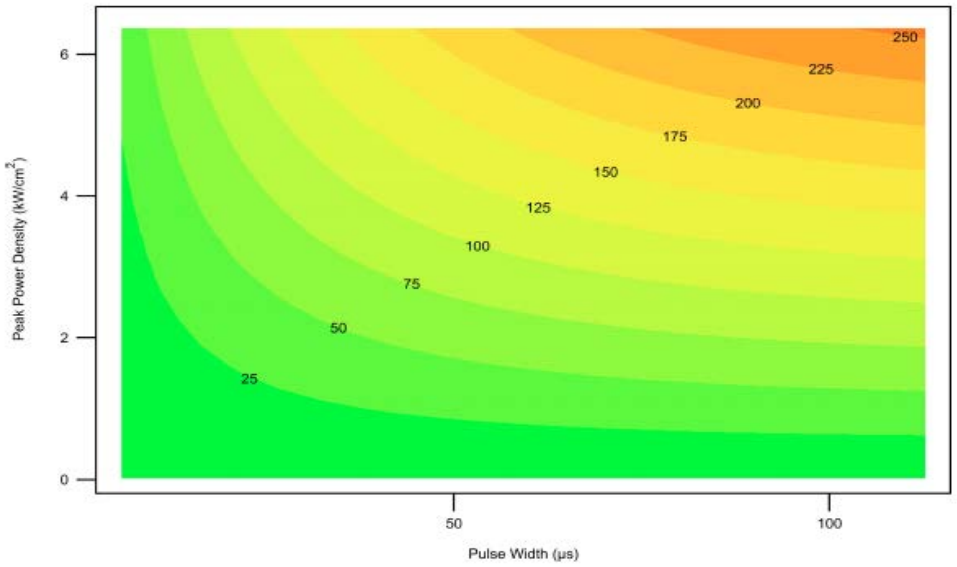


Figure 13. Graphs for ΔT above the array temperature for an average areal power density of 25W/cm$^2$[15]

The graph above shows ΔT above the array temperature for different peak powers and duty cycles for DLP 550 XGA S450. With a peak power density of *7.85kW/cm$^2$* and a pulse width of *25ns* , one can predict from the graph that the temperature rise is not going to exceed *25 °C* or a more conservative estimate, say it's not going to exceed *50 °C* at any cost. Thus, according to the formula, the max. temperature of the pixel can be at the most *60+50=110°C* (this is an over-conservative estimate) which is lower than *150 °C*.

| ΔT TO ARRAY | 100 Hz | | 1 kHz | | 10 kHz | |
|---|---|---|---|---|---|---|
| PACKAGE | 25% DC (1/4) [2.5 ms pulse] | 0.098% DC (1/1024) [9.78 µs pulse] | 25% DC (1/4) [250 µs pulse] | 0.098% DC (1/1024) [978 ns pulse] | 25% DC (1/4) [25 µs pulse] | 0.098% DC (1/1024) [97.8 ns pulse] |
| 0.7-inch (17.78-mm) XGA (A) | 5.3°C | 225°C | 5.2°C | 24.4°C | 2.3°C | 3.0°C |
| 0.95-inch (24.13-mm) 1080p (A) | 4.4°C | 217°C | 4.3°C | 23.8°C | 2.1°C | 2.7°C |
| 0.55-inch (13.97-mm) XGA (S450) | 4.4°C | 217°C | 4.3°C | 23.8°C | 2.1°C | 2.7°C |

Table 5. Table showing Peak pixel temperature for various TI packages at different repetition rates with 25% and 0.098% duty cycle for an average areal power density of 25W/cm$^2$[15]

Following can be observed by looking at table 5.

1. At same duty cycle and lower pulse durations, the temperature rise is smaller.
2. At same repetition rate, smaller duty cycles result in higher temperature rise.

Based on these two observations, one can conclude that at *100KHz* , the ΔT for *25%* duty cycle would be less than *2.1 °C* and for *0.098%* duty cycle, it would be less than *2.7°C*. And, thus for Talon 532-20 (*100KHz, 0.25% duty cycle, 25ns pulse duration*) , the temperature rise would definitely be lower than *2.7 °C*. Thus, the overall pixel temperature is not going anywhere

close to *150 °C* and hence, the chipset should be safe to use for this application with the above stated laser.

**Throughput Calculations**

One major drawback with the light engine is that the laser loses *70-80%* of its energy till it reaches the target and that can reduce the throughput significantly. Assuming that the laser loses *90%* of its energy till it reaches the powder bed (this is worst case scenario.Typically, it loses around *75-80%* energy). So,

Total energy reaching the powder bed= *1.8W*;
Energy per pulse reaching the powder bed= $1.8 * 10^{-5} J$;
Energy per pulse per mirror = $1.8 * 10^{-5}/786432 = 2.29 * 10^{-11} J$;
Energy required to sinter a spot of $1\mu m$ diameter and $1\mu m$ thickness= $4.83 * 10^{-9} J$;
Total no. of pulses required to sinter the spot = $4.83 * 10^{-9}/(2.29 * 10^{-11}) = 211$;
At *100KHz, 211 pulses= 0.00211s*;
Total volume sintered in *1s*= $786432 * (10^{-6}) * \pi * 10^{-6} * 10^{5}/(4 * 211)\ m^3$;
Volumetric throughput = $2.93 * 10^{-4}$ *ml/s= 1.0537 ml/hr*;
Areal scan rate (assuming a $1\mu m$ thick layer) =$293 mm^2/s$

Suppose, the wafers are *2" by 2"* in size and desired thickness of Cu on the substrate is *1$\mu m$*. With this system, 420 such wafers can be sintered in an hour. Though, this doesn't take into account other times involved in wafer installation, stepping action of light engine (which will reduce the throughput ) but it is still much better as compared to the traditional optics system.


Figure 14. CEL 5500 Light Engine[17]

## Conclusion

The study has presented a detailed holistic design for a Selective Laser Sintering system that can be used for sintering micro-scale features. Though the powder spreader is designed so that agglomeration is minimal but it is still significant and largely affects the powder density and uniformity in the layer which in turn will affect the material properties of the sintered part. In order to mitigate the problem of agglomeration among the powders, we are looking into the idea of using nanocopper inks (which are Cu NPs dispersed in an organic solvent like ethylene glycol). These nanocopper inks have a great advantage over nanopowders in terms of significantly lower agglomeration among the particles and also lesser chances of oxidation and hence, they can be sintered in a low vacuum environment as well thus relaxing the vacuum requirements. Further studies will present a detailed analysis of the usage of copper nanoinks for sintering.

## References


1. Yuan, M., D. Bourell, and T. Diller. *Thermal conductivity measurements of polyamide 12*. in *In Proceedings of the Solid Freeform Fabrication Symposium*. 2011.
2. Exner, H., et al. *Selective laser micro sintering with a novel process*. in *Fourth International Symposium on Laser Precision Microfabrication*. 2003. International Society for Optics and Photonics.
3. Dewidar, M.M.A., *Direct and indirect laser sintering of metals*, 2002, University of Leeds.
4. Regenfuss, P., et al., *Microparts by a novel modification of selective laser sintering.*
5. Ebert, R., et al. *Process assembly for µm-scale SLS, reaction sintering, and CVD*. in *Fourth International Symposium on laser Precision Microfabrication*. 2003. International Society for Optics and Photonics.
6. Streek, A., et al. *Laser micro sintering–a quality leap through improvement of powder packing*. in *The Proceedings of the 19th Annual SFF Symposium*. 2008.
7. Eco Blade, I., *Eco Blade offers the finest in custom-made doctor blades*, 2015: Yokohama, Japan.
8. Pfeifer Industries, L. *Timing Belt Advantages and Disadvantages*. 2015 [cited 2015.
9. Lahmadi, W., *VSS Stepper Motor: For applications upto ultra-high vacuum*, I. Phytron, Editor 2015.
10. Biltoft, P. and M. Benapfl, *Vacuum Technology.* Theory and Laboratory Exercises, Las Positas College, 2002: p. 126.
11. Gmbh, P.V., *HiCube Eco*.
12. Instruments, T., *DLP 5500 DLP 0.55 XGA Series 450 DMD*, May 2015.
13. Jang, S., et al., *Sintering of inkjet printed copper nanoparticles for flexible electronics.* Scripta Materialia, 2010. **62**(5): p. 258-261.
14. Tolochko, N.K., et al., *Absorptance of powder materials suitable for laser sintering.* Rapid Prototyping Journal, 2000. **6**(3): p. 155-161.
15. Instruments, T., *Laser Power Handling for DMDs*, January 2012.
16. Instruments, T., *DLP Series-450 DMD and System Mounting Concepts*, June 2010.
17. Innovations, D.L., C. 5500, Editor 2014.
18. Kumar, S., *Selective laser sintering: a qualitative and objective approach.* JOM, 2003. **55**(10): p. 43-47.
19. Das, S., *Physical aspects of process control in selective laser sintering of metals.* Advanced Engineering Materials, 2003. **5**(10): p. 701-711.